The impact of NO_x addition on the ignition behavior of n-pentane Supplemental Material - Additional Figures and Tables

Mark E. Fuller*[a‡], Philipp Morsch[a], Matthias Preußker[a], C. Franklin Goldsmith[b], and K. Alexander Heufer[a]

Additional notes on supplemental materials:

- The preprint of this manuscript, including supplemental materials, is available at `https://doi.org/10.26434/chemrxiv.13720105`
- The v.0 mechanism has been deposited into an open database at `https://github.com/jiweiqi/CollectionOfMechan` `tree/master/Nitrogen/Fuller-2021`
- The experimental data files have been deposited into an open database at `https://github.com/pr-omethe-us/ChemKED-database`

References

1 J. Bugler, B. Marks, O. Mathieu, R. Archuleta, A. Camou, C. Grégoire, K. A. Heufer, E. L. Petersen and H. J. Curran, *Combustion and Flame*, 2016, **163**, 138–156.

2 P. Glarborg, J. A. Miller, B. Ruscic and S. J. Klippenstein, *Progress in Energy and Combustion Science*, 2018, **67**, 31–68.

3 L. Marrodán, Y. Song, M. L. Lavadera, O. Herbinet, M. de Joannon, Y. Ju, M. U. Alzueta and F. Battin-Leclerc, *Energy & Fuels*, 2019, **33**, 5655–5663.

[a] *Physico-Chemical Fundamentals of Combustion, RWTH Aachen University, 52062 Aachen Germany; E-mail: fuller@pcfc.rwth-aachen.de*

[b] *School of Engineering, Brown University, Providence, RI 02912, USA*

‡ Present address: Faculty of Chemical Engineering, Technion I.I.T., Haifa 3200003, Israel

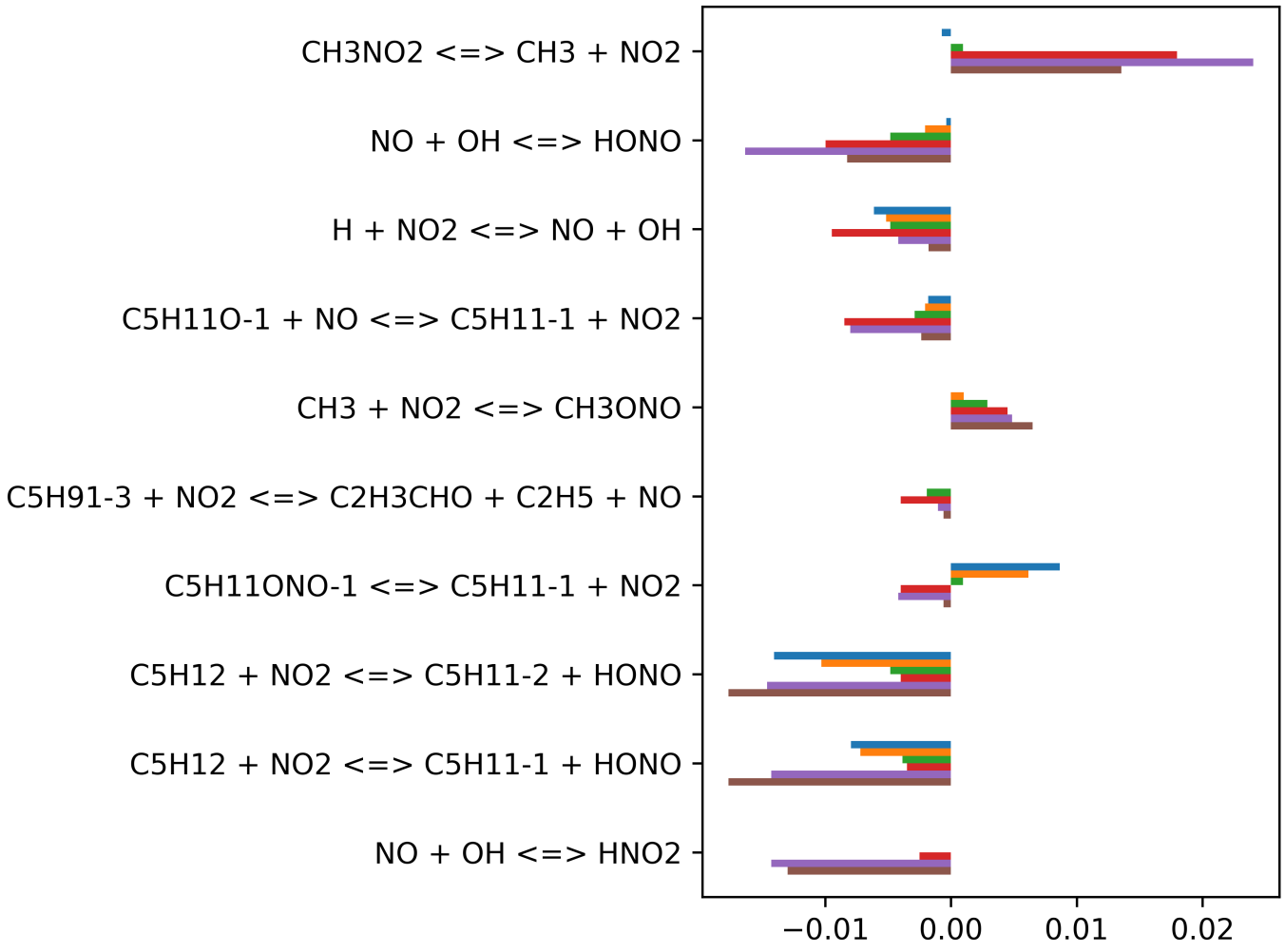

Fig. S1 Sensitivities $\left(\frac{\partial \ln \tau}{\partial \ln k}\right)$ among reactions added to the mechanisms of Bugler *et al.*[1] and Glarborg *et al.*[2] for *n*-pentane in synthetic air diluted with N_2 at equivalence ratio of ϕ = 1.0 with 333 ppm NO_2. Individual bands represent analysis at temperatures of 650 K (top, blue) to 900 K (bottom, brown) in 50 K increments.

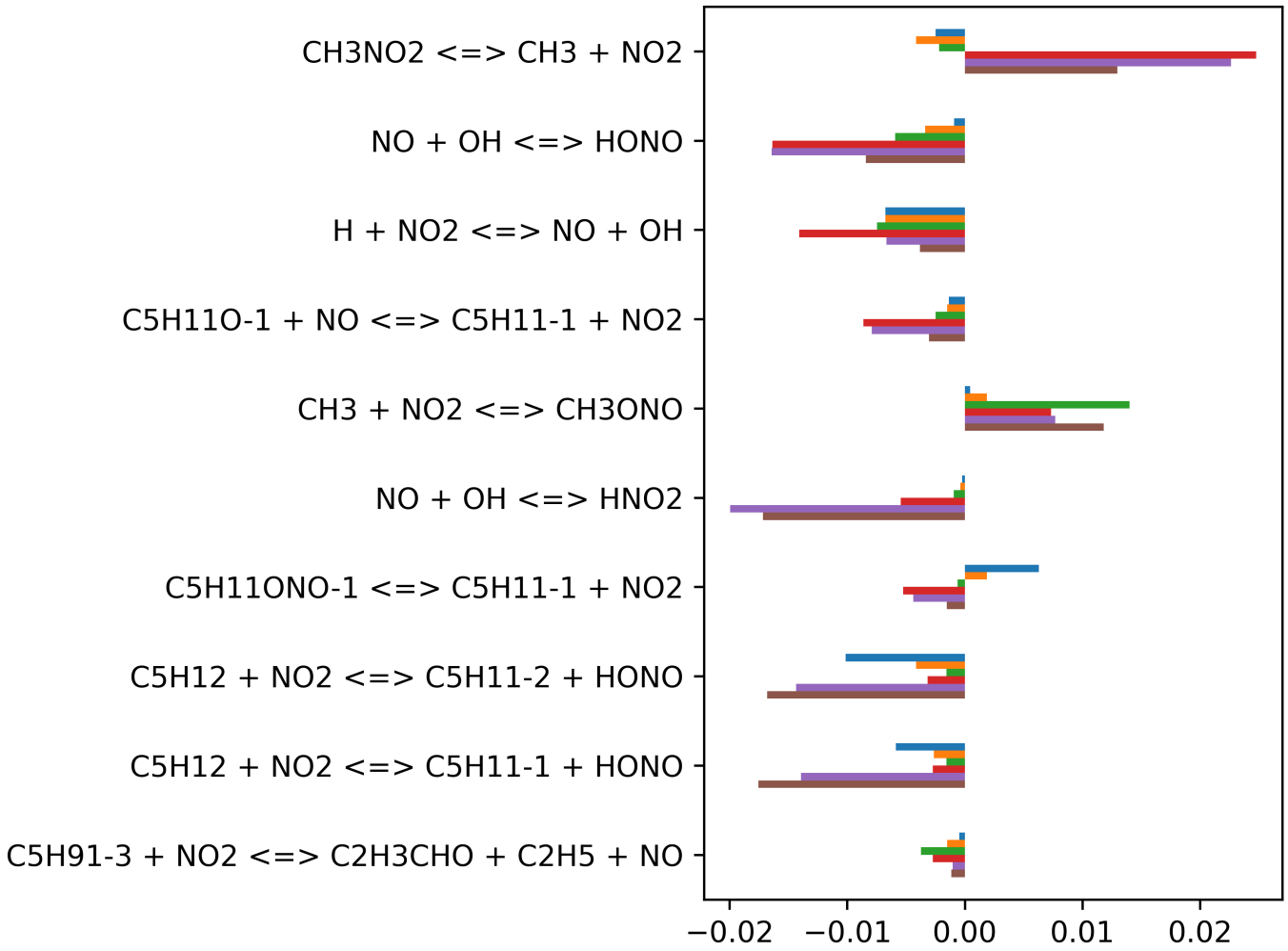

Fig. S2 Sensitivities $\left(\frac{\partial \ln \tau}{\partial \ln k}\right)$ among reactions added to the mechanisms of Bugler *et al.*[1] and Glarborg *et al.*[2] for *n*-pentane in synthetic air diluted with N_2 at equivalence ratios of ϕ = 0.5 with 333 ppm NO_2. Individual bands represent analysis at temperatures of 650 K (top, blue) to 900 K (bottom, brown) in 50 K increments.

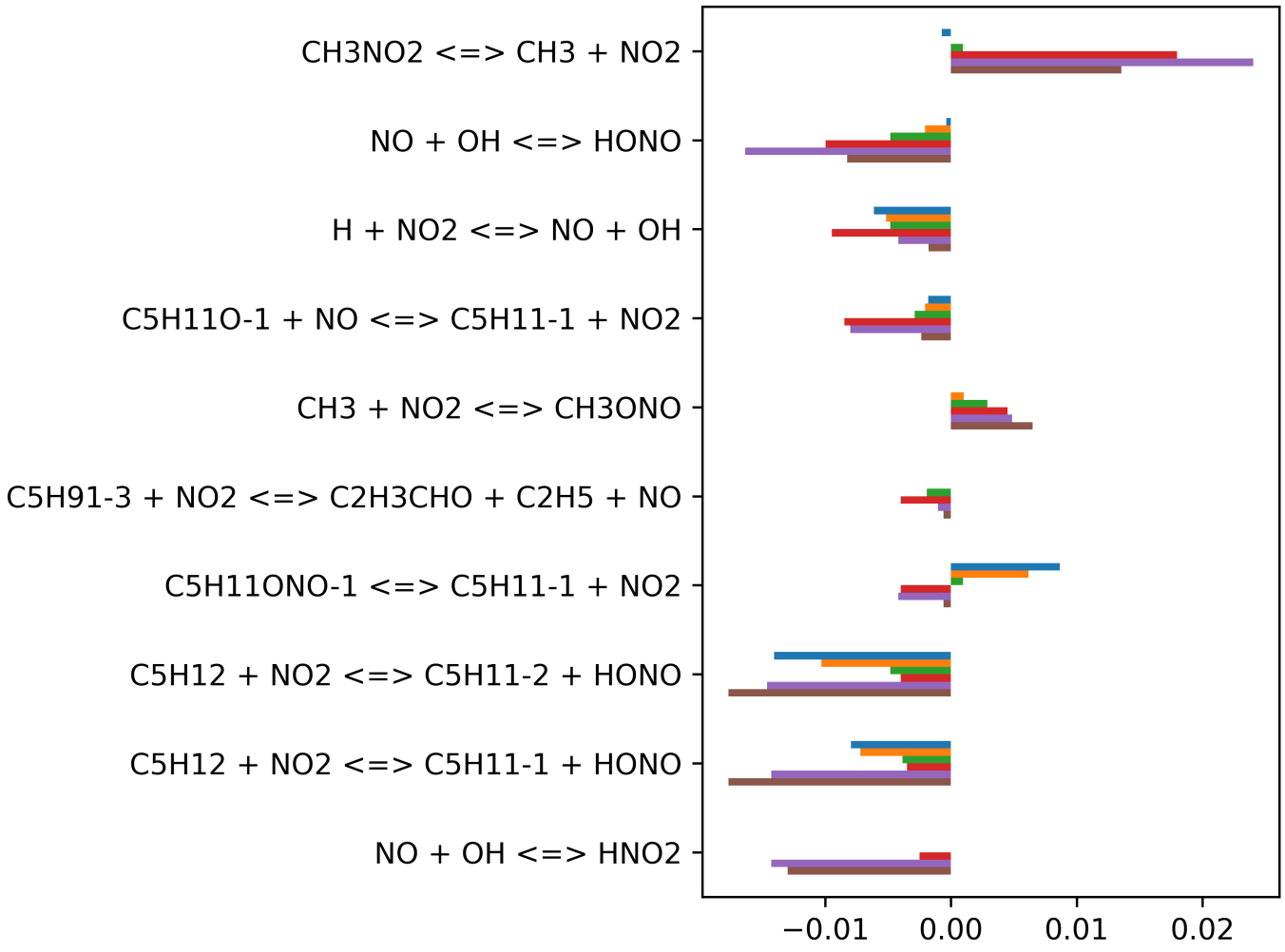

Fig. S3 Sensitivities $\left(\frac{\partial \ln \tau}{\partial \ln k}\right)$ among reactions added to the mechanisms of Bugler *et al.*[1] and Glarborg *et al.*[2] for *n*-pentane in synthetic air diluted with N_2 at equivalence ratios of ϕ = 2.0 with 333 ppm NO_2. Individual bands represent analysis at temperatures of 650 K (top, blue) to 900 K (bottom, brown) in 50 K increments.

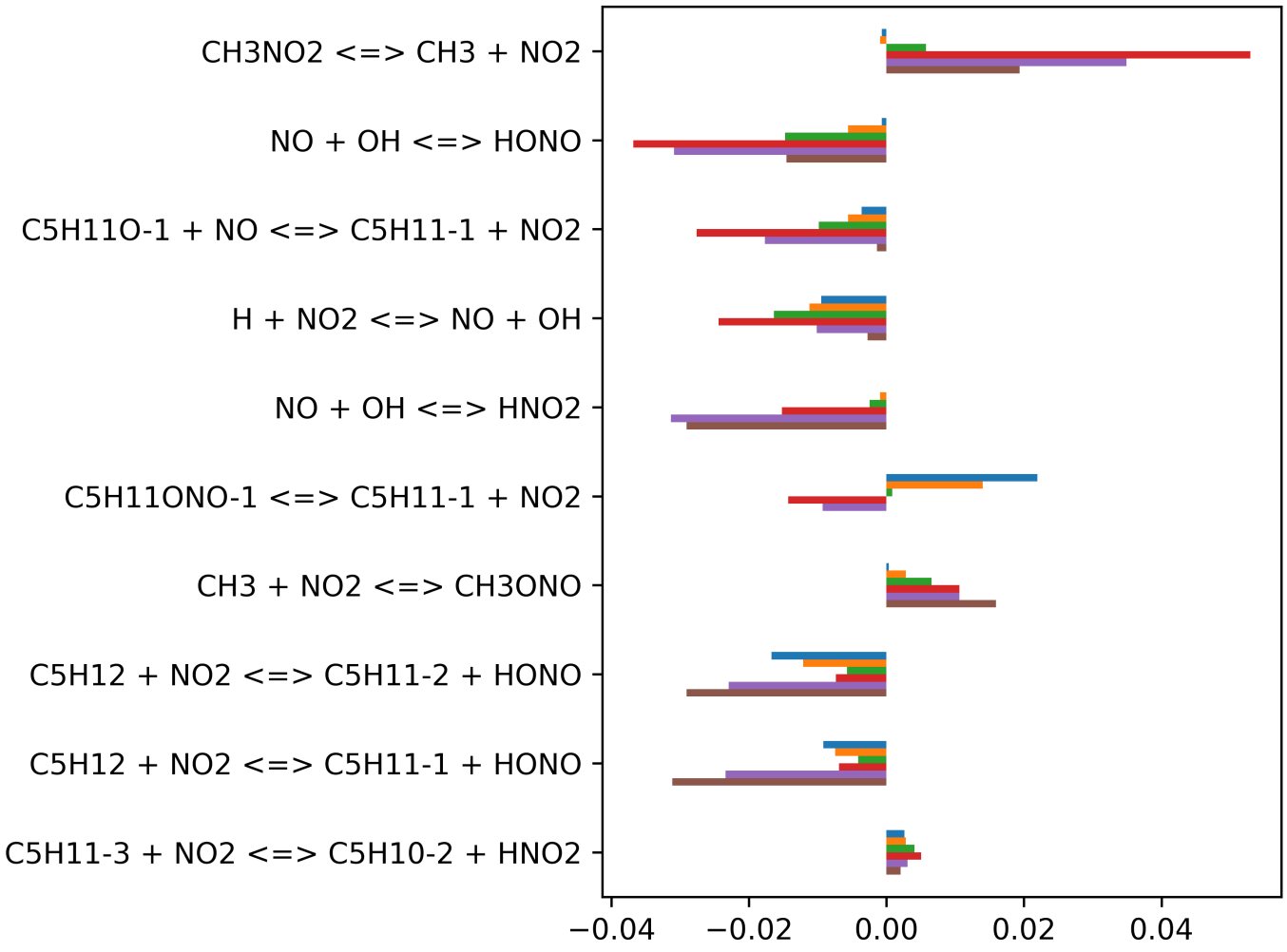

Fig. S4 Sensitivities $\left(\frac{\partial \ln \tau}{\partial \ln k}\right)$ among reactions added to the mechanisms of Bugler *et al.*[1] and Glarborg *et al.*[2] for *n*-pentane in synthetic air diluted with N_2 at equivalence ratios of ϕ = 1.0 with 1000 ppm NO_2. Individual bands represent analysis at temperatures of 650 K (top, blue) to 900 K (bottom, brown) in 50 K increments.

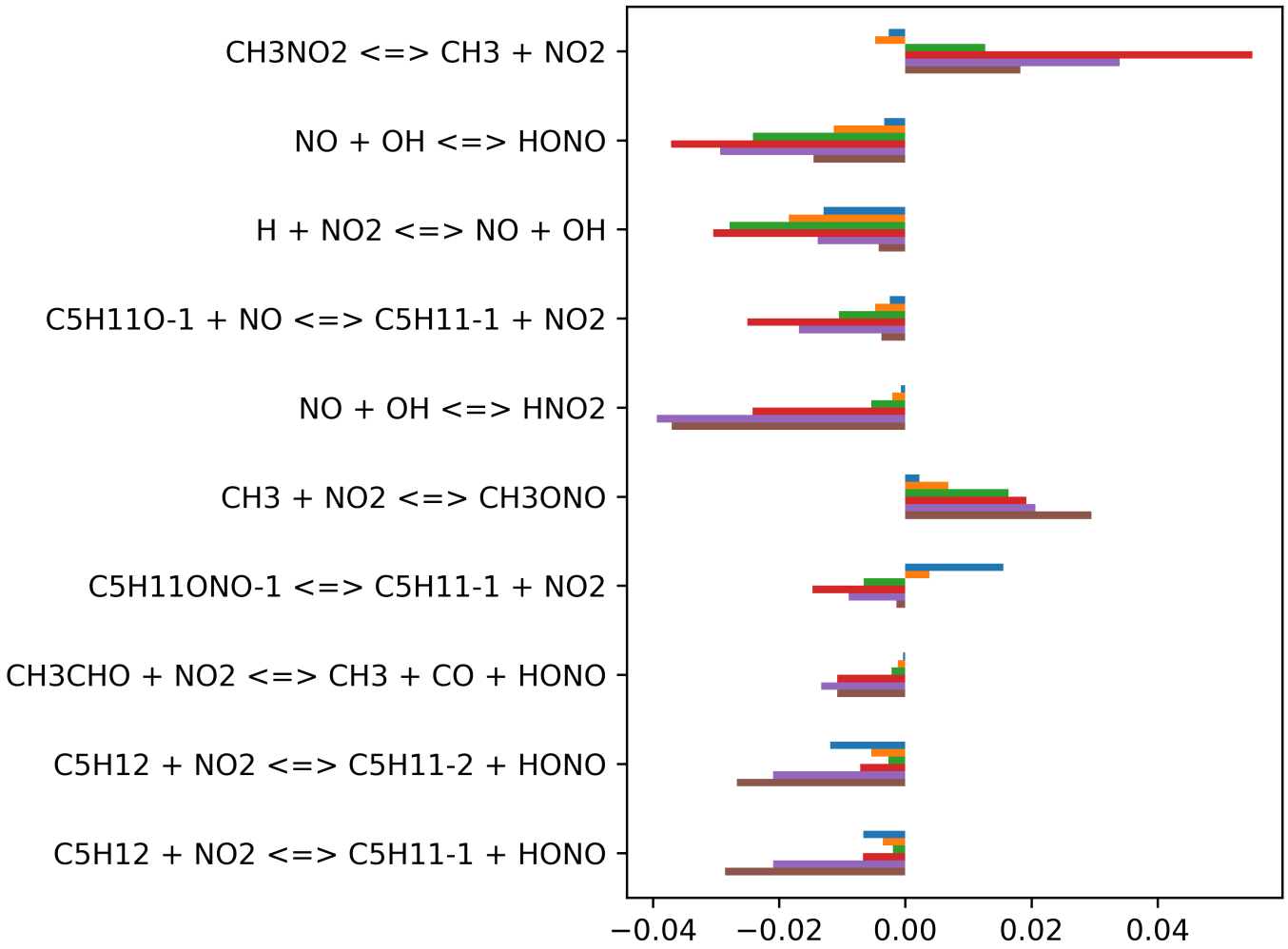

Fig. S5 Sensitivities $\left(\frac{\partial \ln \tau}{\partial \ln k}\right)$ among reactions added to the mechanisms of Bugler *et al.*[1] and Glarborg *et al.*[2] for *n*-pentane in synthetic air diluted with N_2 at equivalence ratios of ϕ = 0.5 with 1000 ppm NO_2. Individual bands represent analysis at temperatures of 650 K (top, blue) to 900 K (bottom, brown) in 50 K increments.

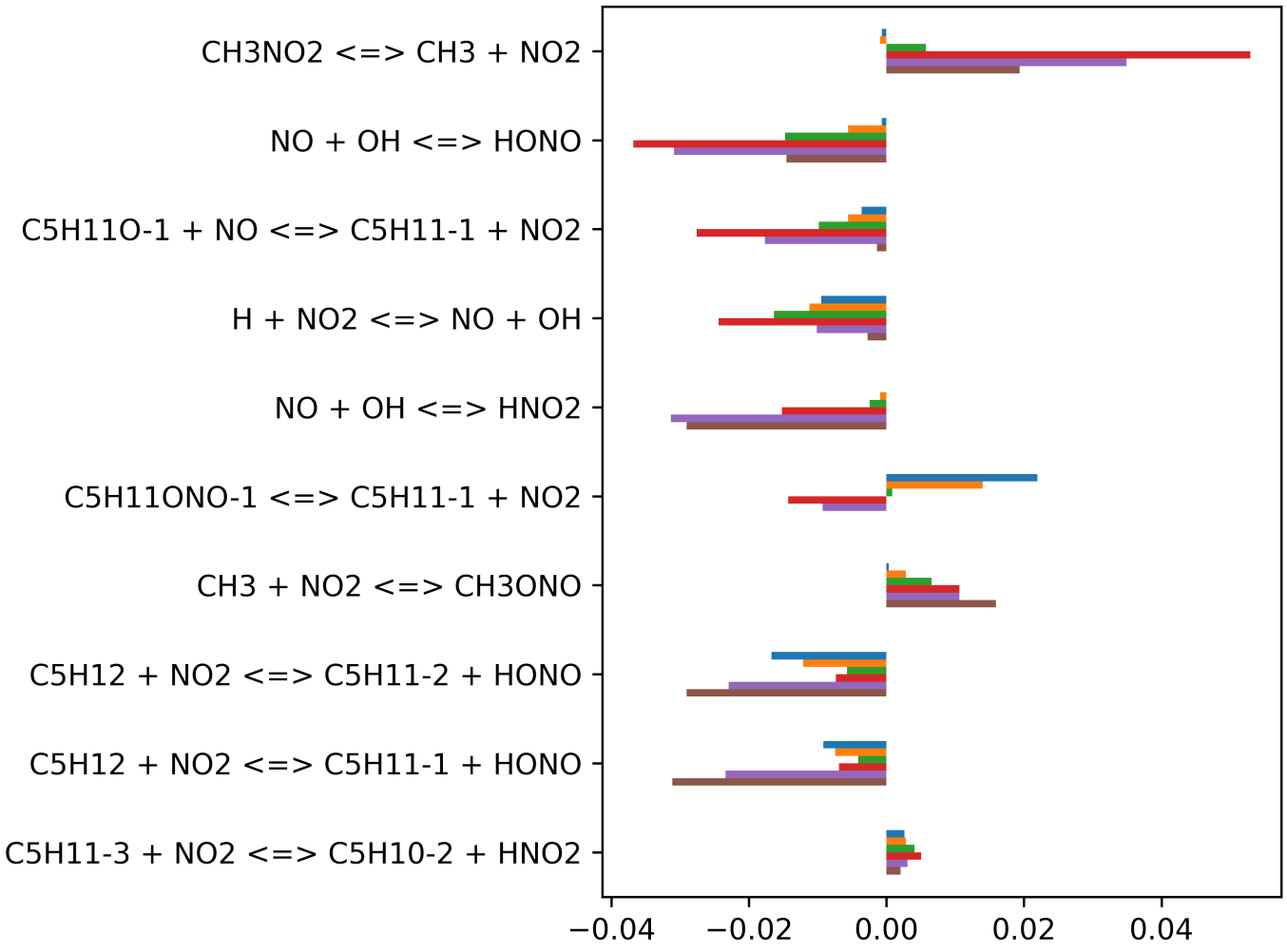

Fig. S6 Sensitivities $\left(\frac{\partial \ln \tau}{\partial \ln k}\right)$ among reactions added to the mechanisms of Bugler *et al.*[1] and Glarborg *et al.*[2] for *n*-pentane in synthetic air diluted with N_2 at equivalence ratios of ϕ = 2.0 with 1000 ppm NO_2. Individual bands represent analysis at temperatures of 650 K (top, blue) to 900 K (bottom, brown) in 50 K increments.

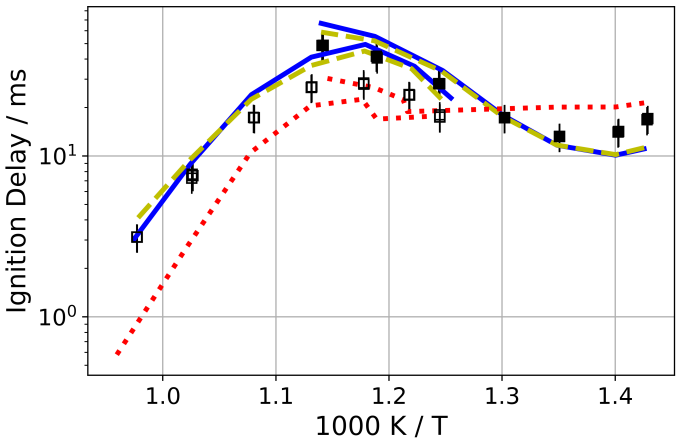

(a) ϕ = 1.0; 333 ppm NO_2

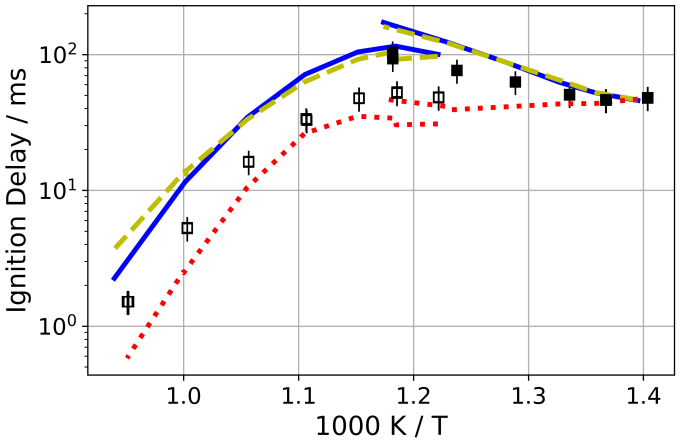

(b) ϕ = 0.5; 333 ppm NO_2

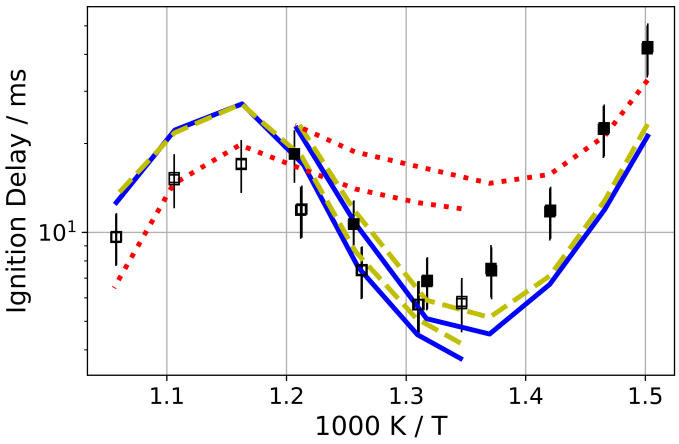

(c) ϕ = 2.0; 333 ppm NO_2

Fig. S7 Model predictions for n-pentane in synthetic air diluted with N_2 or Ar at equivalence ratios of ϕ = 1.0, 0.5, 2.0 and with 333 ppm NO_2. Closed symbols are experiments conducted with N_2 diluent; open symbols are Ar diluent. The solid blue line is the v.0 model presented in this work and the dashed yellow line is the v.1 optimized version with improved rate rules. The red dotted line is the model of Marrodán *et al.*[3].

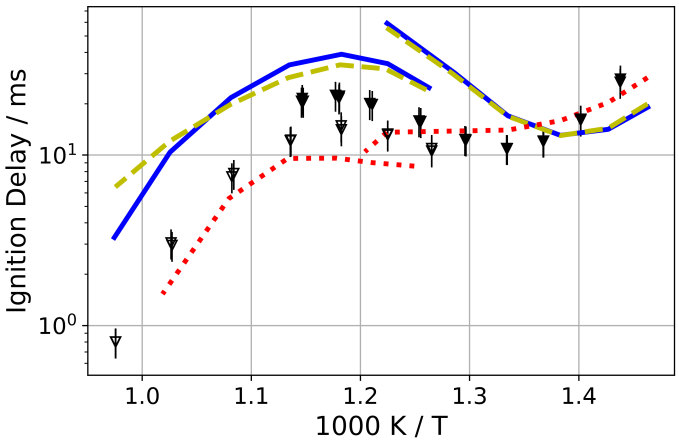

(a) ϕ = 1.0; 1000 ppm NO

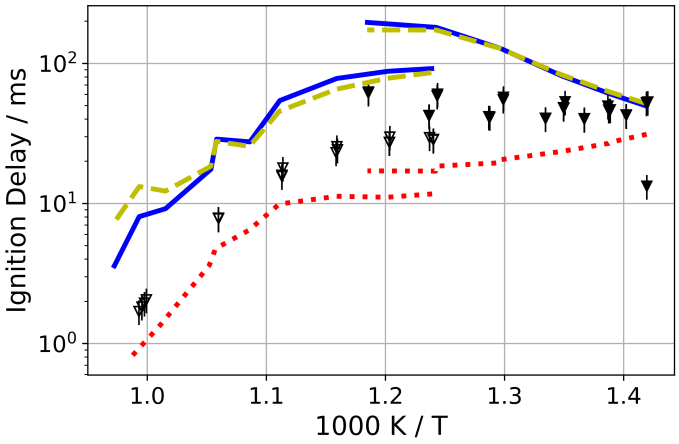

(b) ϕ = 0.5; 1000 ppm NO

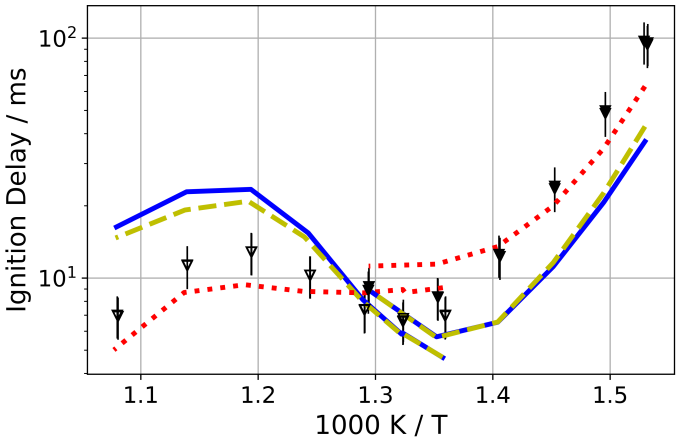

(c) ϕ = 2.0; 1000 ppm NO

Fig. S8 Model predictions for n-pentane in synthetic air diluted with N_2 or Ar at equivalence ratios of ϕ = 1.0, 0.5, 2.0 and initially doped with 1000 ppm NO, fully reacted with O_2 to NO_2 by the start of the experiment. Closed symbols are experiments conducted with N_2 diluent; open symbols are Ar diluent. The solid blue line is the v.0 model presented in this work and the dashed yellow line is the v.1 optimized version with improved rate rules. The red dotted line is the model of Marrodán *et al.*[3].

As a further effort to validate our assumption of complete conversion of NO to NO_2 in the mixing vessel through comsumption of molecular oxygen, *i.e.* $NO + 0.5O_2 \rightleftharpoons NO_2$, a reference data set of IDT experiments containing 1000 ppm NO was compared with a second data set where NO was replaced by NO_2 and the O_2 concentration was reduced by 500 ppm, as depicted in figure S10.

The observed ignition delay times of these two mixtures are clearly within their experimental uncertainty, which justifies the assumption of a complete conversion of NO into NO2 and therefore similar measured IDTs. N. B. The new experiments were performed in a second RCM which is of the same design as the primary instrument used in this work, but with slightly different compression characteristics leading to marginally shorter measured ignition delay times. Accordingly, we have added discussion of this phenomena in the manuscript and both re-analyzed and re-categorized the NO-doped experiments as if the dopant were NO_2. We believe that the analysis and explanation added to the manuscript makes both the experimental conditions and analytical approach clear to the reader.

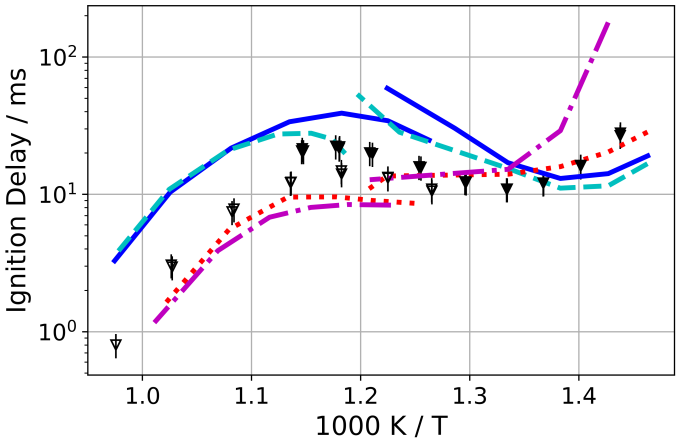

(a) ϕ = 1.0; 1000 ppm NO

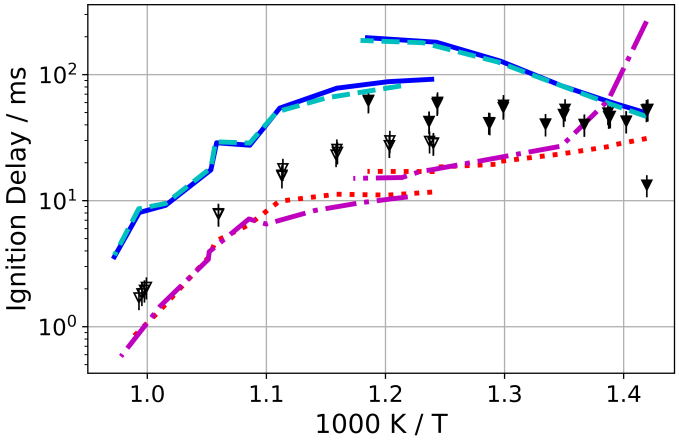

(b) ϕ = 0.5; 1000 ppm NO

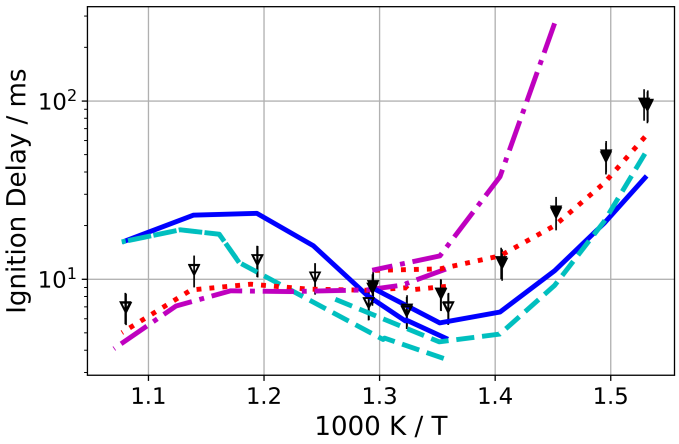

(c) ϕ = 2.0; 1000 ppm NO

Fig. S9 Model predictions for n-pentane in synthetic air diluted with N_2 or Ar at equivalence ratios of ϕ = 1.0, 0.5, 2.0 and initially doped with 1000 ppm NO. Comparison of model predictions resulting from assuming complete conversion of NO to NO_2 via reaction with O_2 and ninety percent conversion prior to the start of the experiment. Closed symbols are experiments conducted with N_2 diluent; open symbols are Ar diluent. The solid blue and dashed cyan lines are the v.0 model presented in this work applied to full and ninety percent conversion of NO to NO_2, respectively. The red dotted and magenta dash-dot lines are the model of Marrodán *et al.*[3] applied to full and ninety percent conversion of NO to NO_2, respectively.

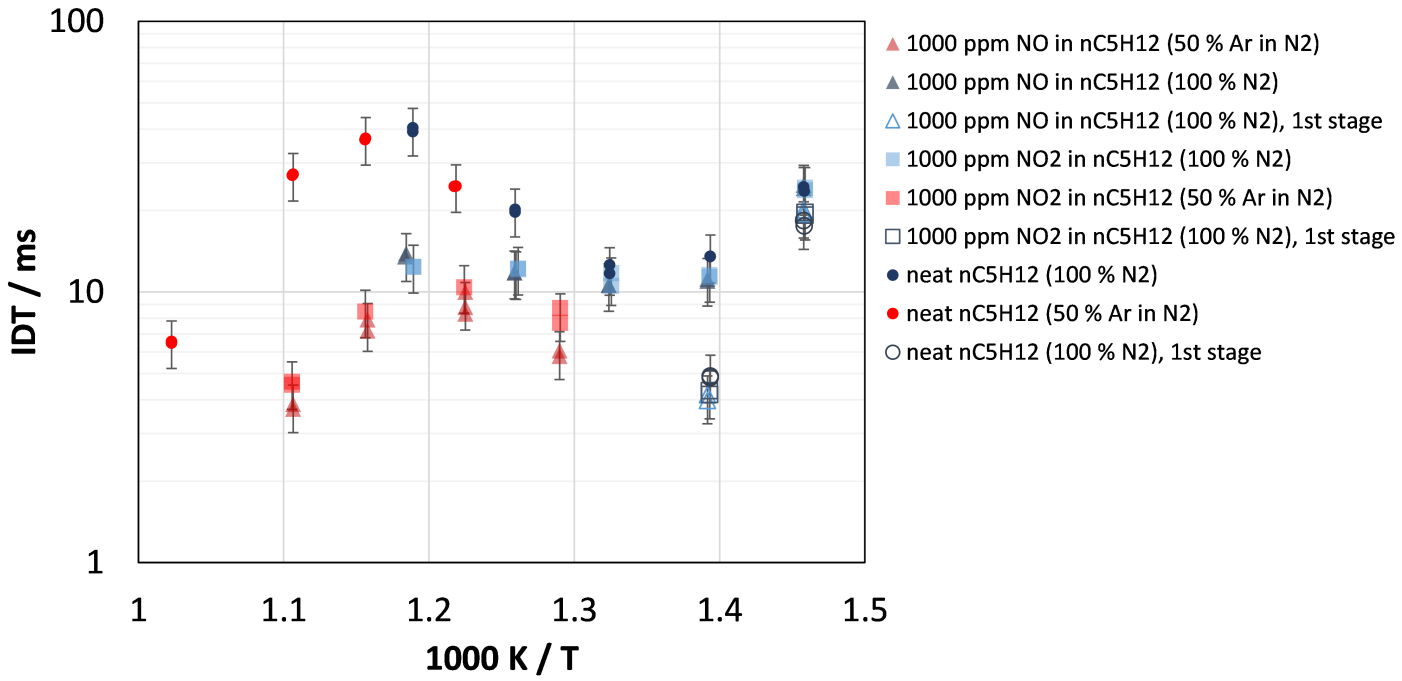

Fig. S10 RCM Ignition Delay Time experiments for neat n-pentane (circles) and n-pentane doped with 1000 ppm NO (triangles) and 1000 ppm NO_2 (squares). pEOC = 15 bar, stoichiometric conditions, X_{DIL}/X_{O_2} = 8.524. Diluent: 100 vol.-% N_2 (blue symbols) and 50 vol.- % Ar/N_2 (red symbols). Open symbols illustrate the first stage of the corresponding experiments.)

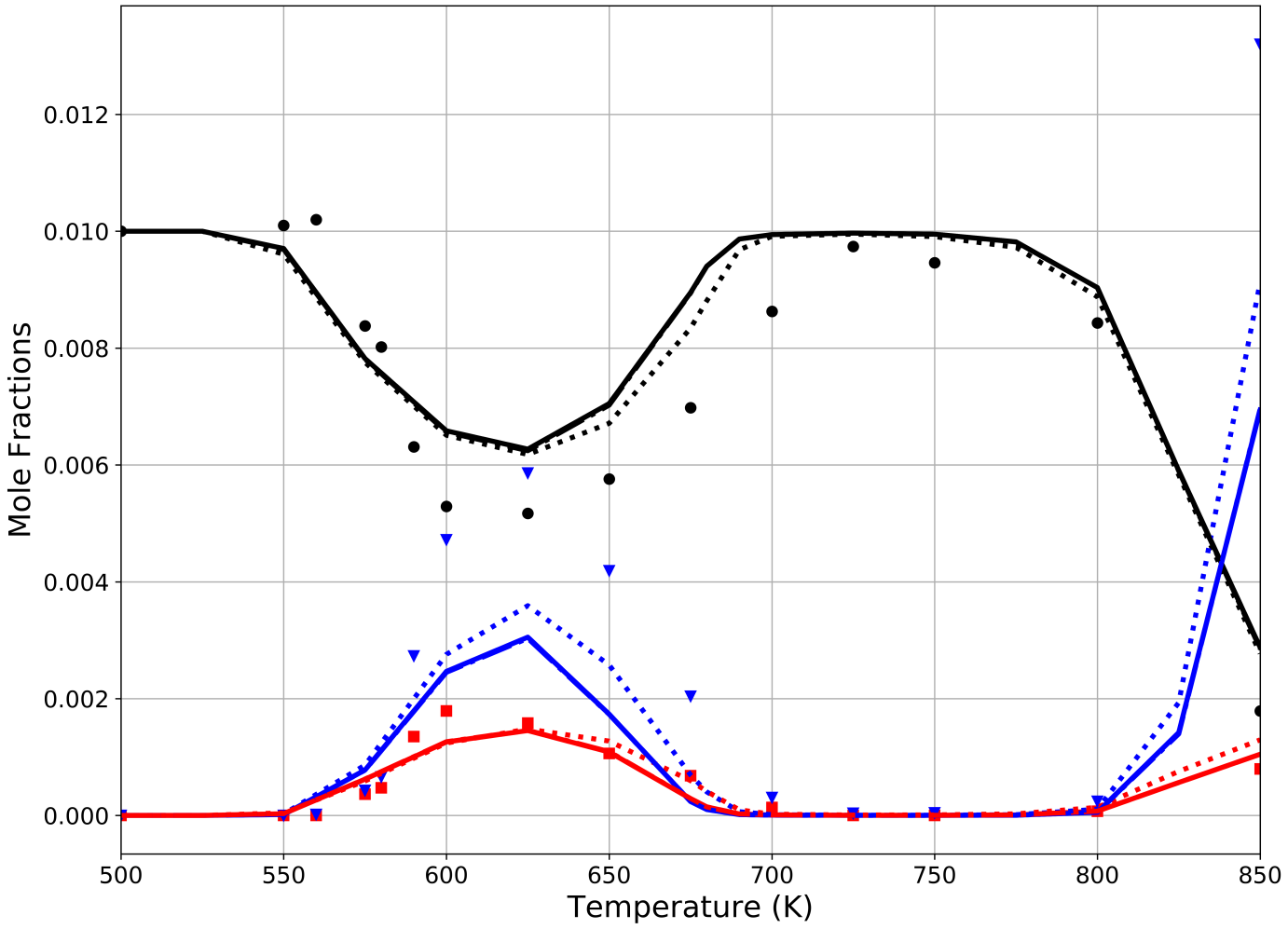

Fig. S11 Comparison of mechanisms for neat pentane oxidation in JSR: Experimental measurements: black circles are n-C_5H_{12}, red squares are CH_2O, blue triangles are CO. The solid lines are the v.0 model presented in this work and the dashed lines are the optimized v.1 model with improved rate rules. The dotted lines are the model of Marrodán *et al.*[3]. The dash-dot lines are the model of Bugler *et al.*[1].

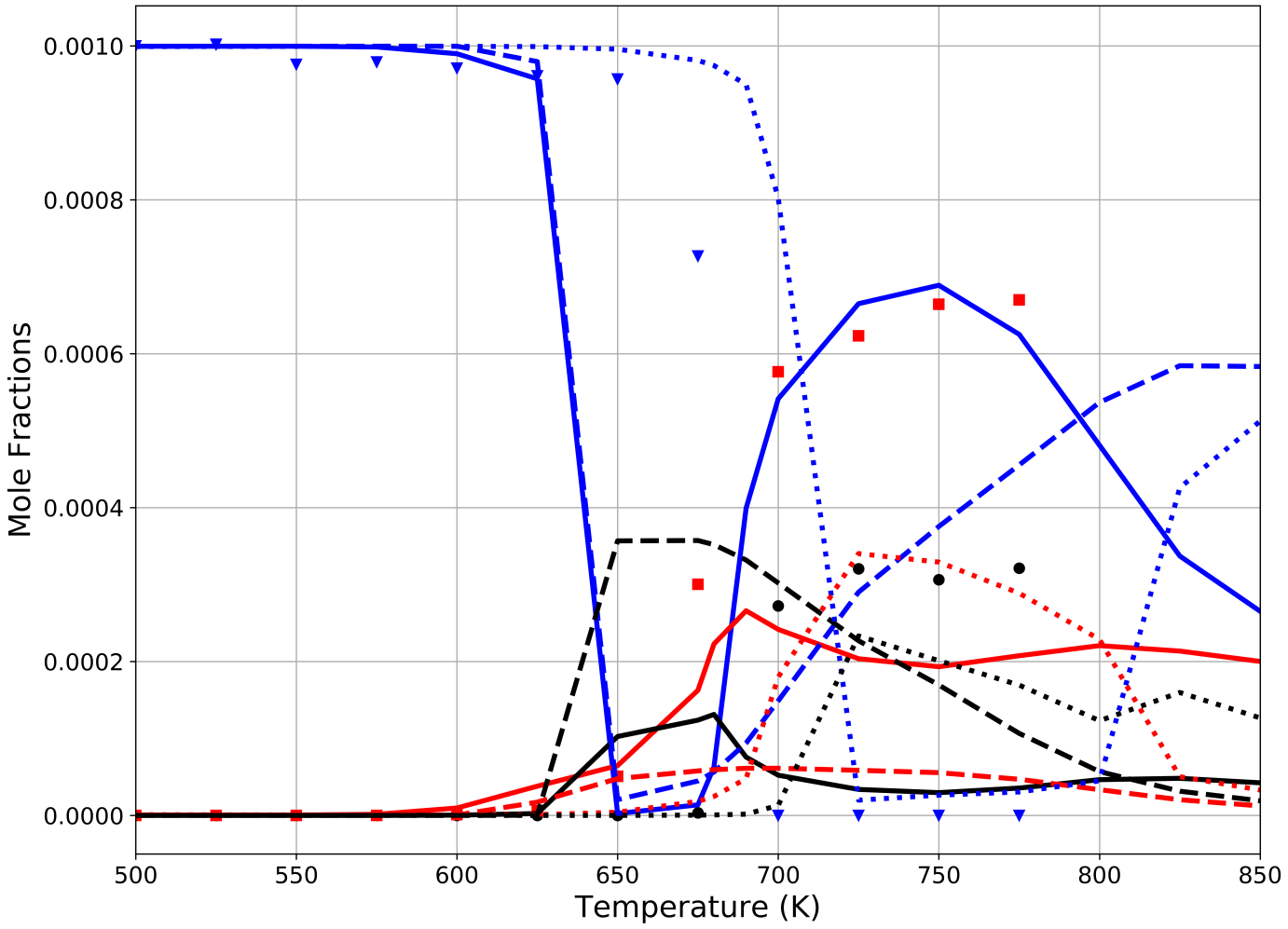

Fig. S12 Comparison of mechanisms for pentane oxidation with 1000 ppm NO in JSR: Experimental measurements: black circles are HONO, red squares are NO_2, blue triangles are NO. The solid lines are the v.0 model presented in this work and the dashed lines are the optimized v.1 model with improved rate rules. The dotted lines are the model of Marrodán *et al.*[3].

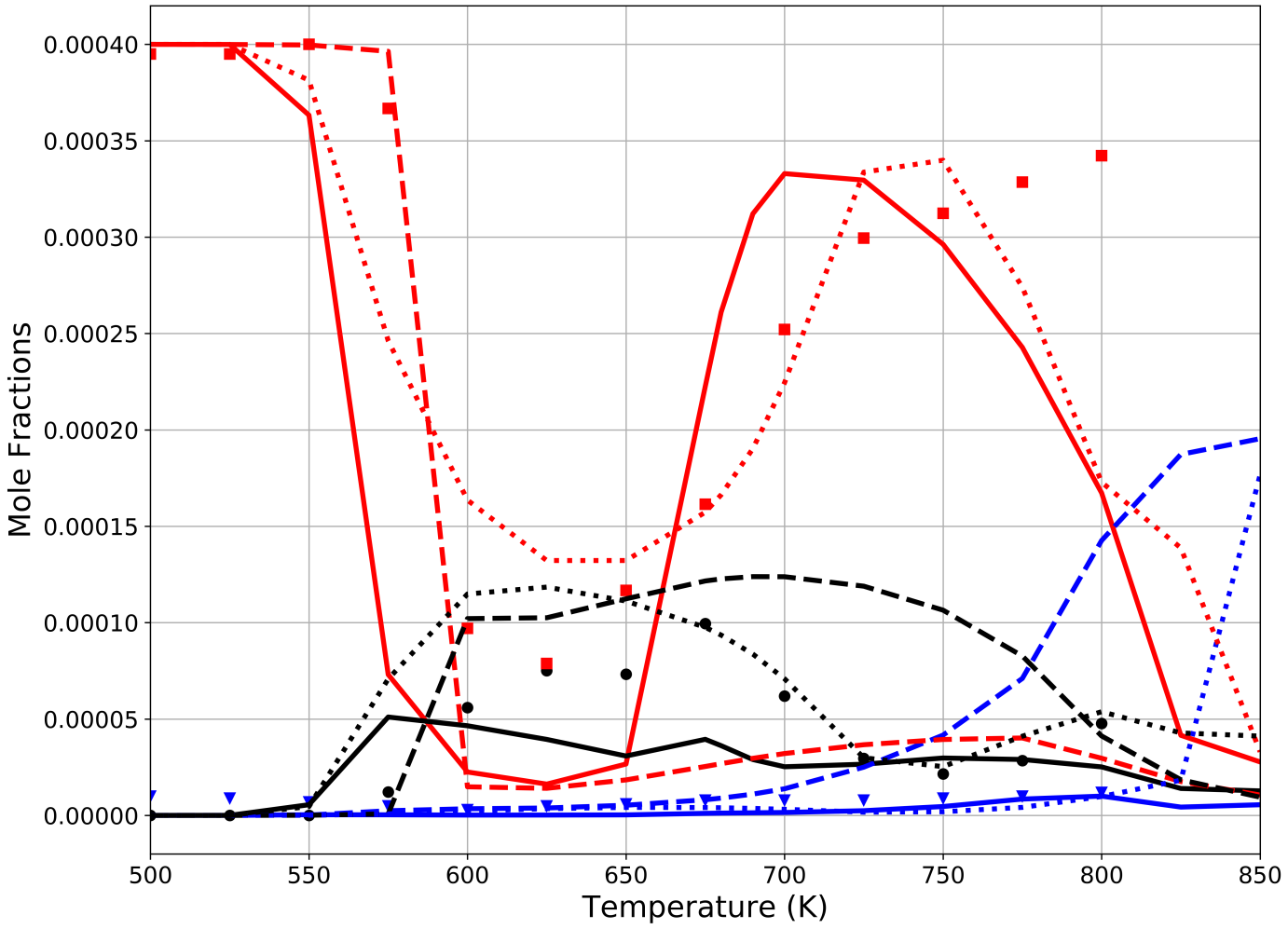

Fig. S13 Comparison of mechanisms for pentane oxidation with 400 ppm NO_2 in JSR: Experimental measurements: black circles are HONO, red squares are NO_2, blue triangles are NO. The solid lines are the v.0 model presented in this work and the dashed lines are the optimized v.1 model with improved rate rules. The dotted lines are the model of Marrodán *et al.* [3].

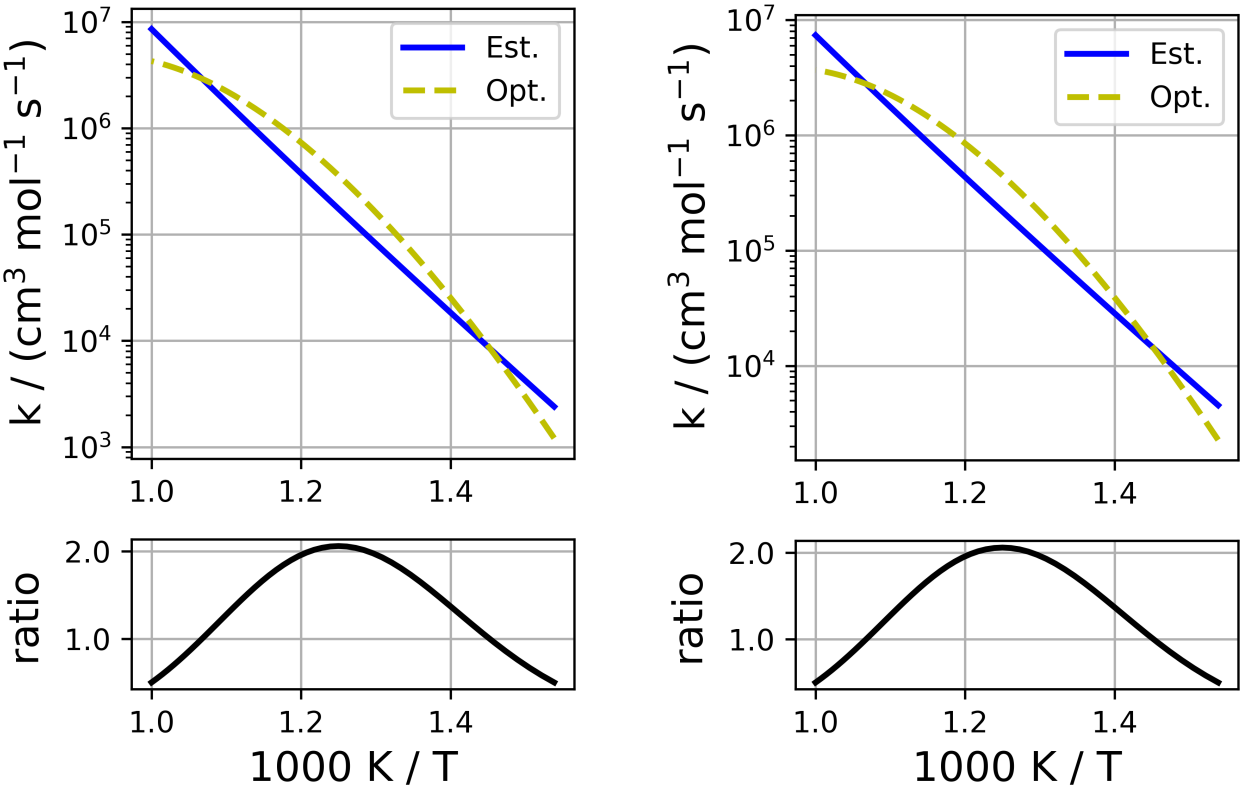

(a) n-C_4H_{10} + NO_2 ⇌ 1-C_4H_9 + HONO

(b) n-C_4H_{10} + NO_2 ⇌ 2-C_4H_9 + HONO

(c) n-C_4H_{10} + NO_2 ⇌ 1-C_4H_9 + HNO_2

(d) n-C_4H_{10} + NO_2 ⇌ 2-C_4H_9 + HNO_2

Fig. S14 Comparison of estimated and optimized rates for hydrogen abstraction reactions of the form RH + NO_2⇌ R + (HONO or HNO_2) for RH = n-C_4H_{10}.

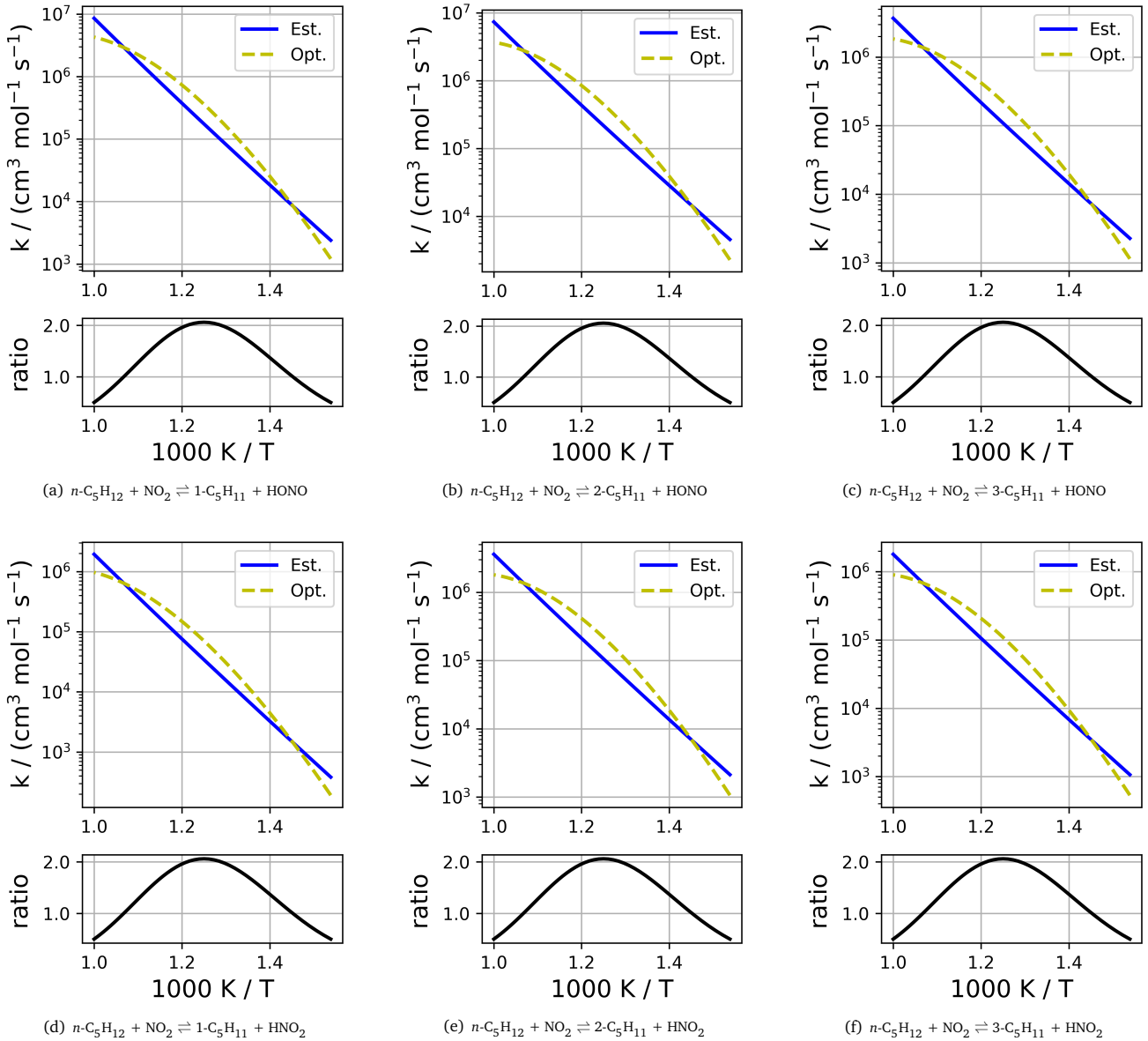

(a) n-C_5H_{12} + NO_2 ⇌ 1-C_5H_{11} + HONO

(b) n-C_5H_{12} + NO_2 ⇌ 2-C_5H_{11} + HONO

(c) n-C_5H_{12} + NO_2 ⇌ 3-C_5H_{11} + HONO

(d) n-C_5H_{12} + NO_2 ⇌ 1-C_5H_{11} + HNO_2

(e) n-C_5H_{12} + NO_2 ⇌ 2-C_5H_{11} + HNO_2

(f) n-C_5H_{12} + NO_2 ⇌ 3-C_5H_{11} + HNO_2

Fig. S15 Comparison of estimated and optimized rates for hydrogen abstraction reactions of the form RH + NO_2⇌ R + (HONO or HNO_2) for RH = n-C_5H_{12}.

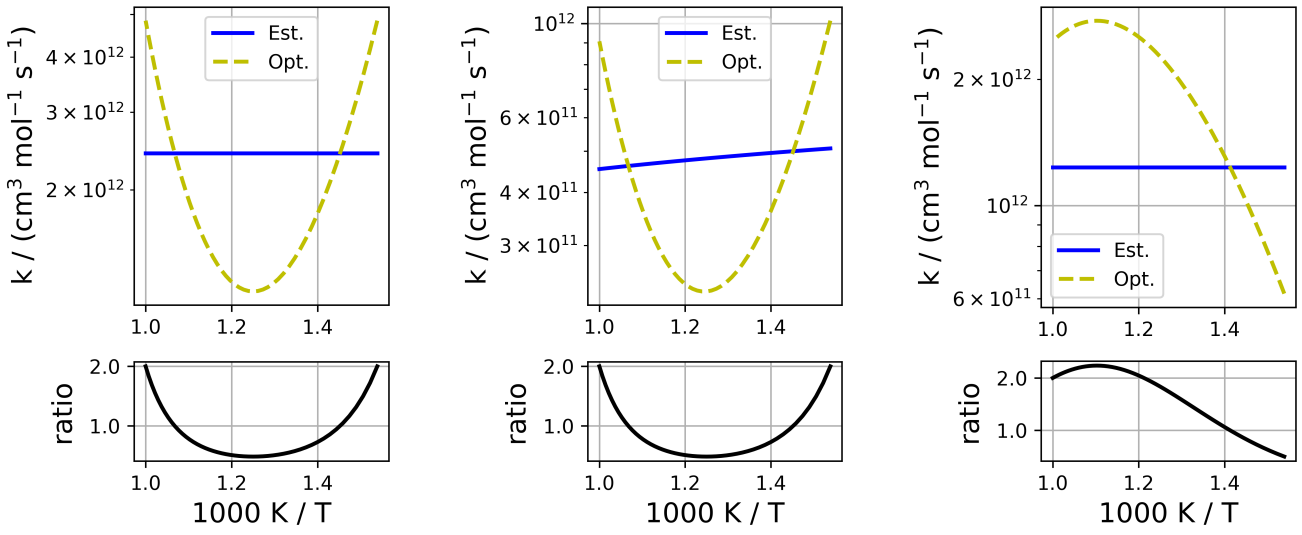

(a) $CH_3 + NO_2 \rightleftharpoons CH_3ONO$ (b) 1-R + $NO_2 \rightleftharpoons$ 1-RONO (c) 2-R + $NO_2 \rightleftharpoons$ 2-RONO

Fig. S16 Comparison of estimated and optimized rates for reactions of the form R + $NO_2 \rightleftharpoons$ RONO.

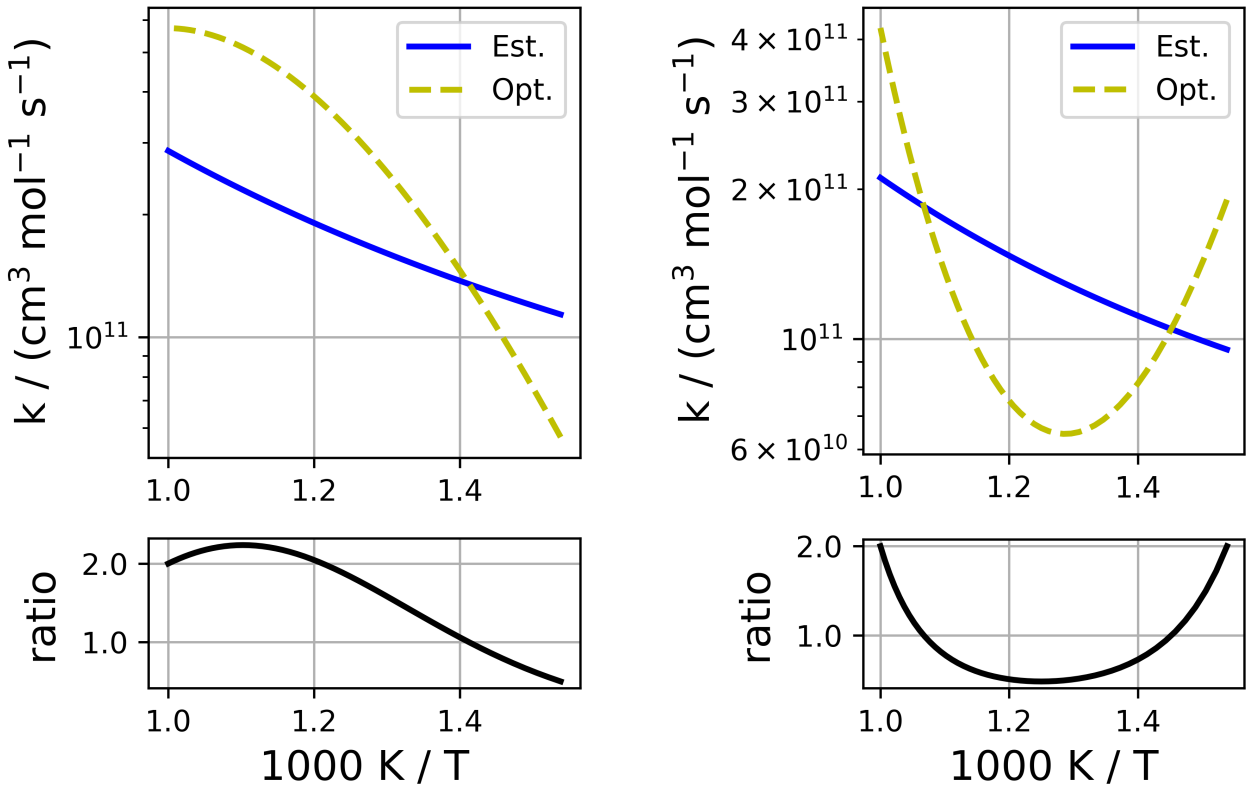

(a) 1-R + HNO $\rightleftharpoons$ *n*-RH + NO (b) 2-R + HNO $\rightleftharpoons$ *n*-RH + NO

Fig. S17 Comparison of estimated and optimized rates for hydrogen abstraction reactions of the form RH + NO$\rightleftharpoons$ R + HNO.

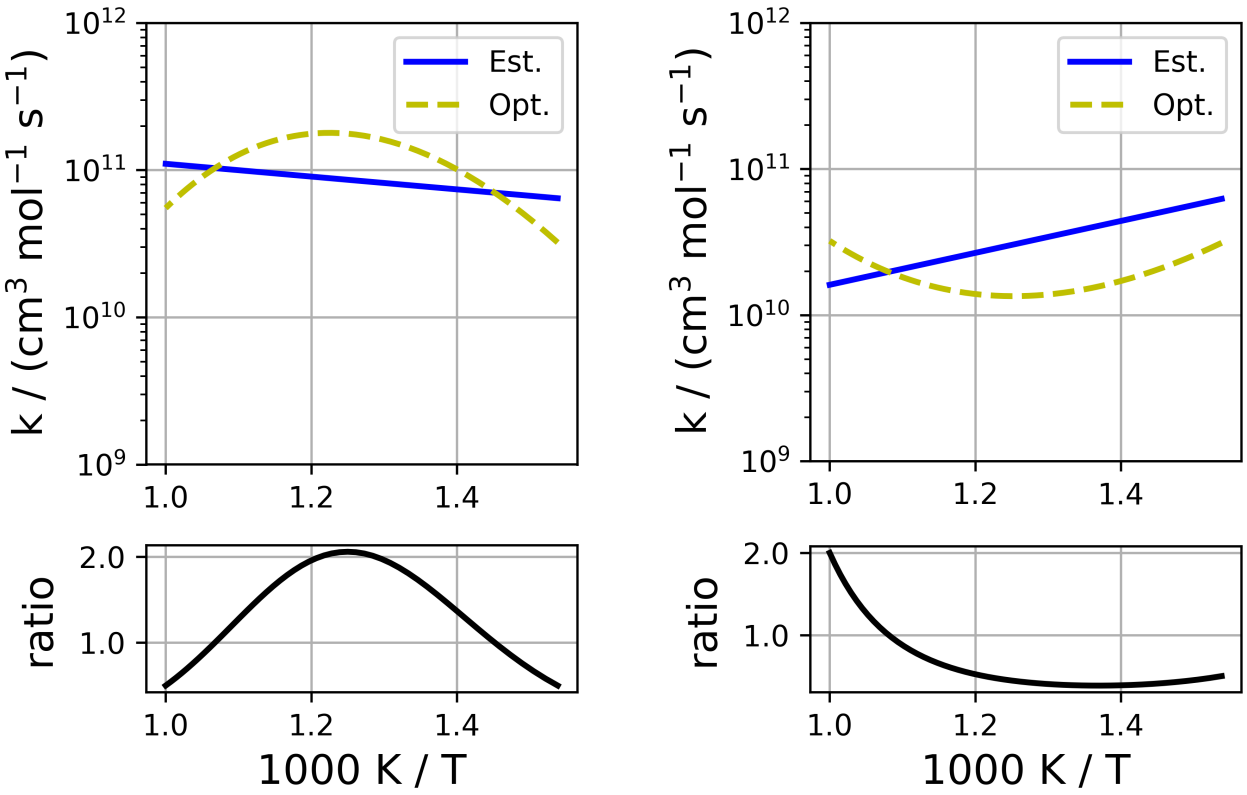

(a) $HNO + NO_2 \rightleftharpoons HNO_2 + NO$

(b) $C_2H_5O_2 + NO \rightleftharpoons C_2H_5O + NO_2$

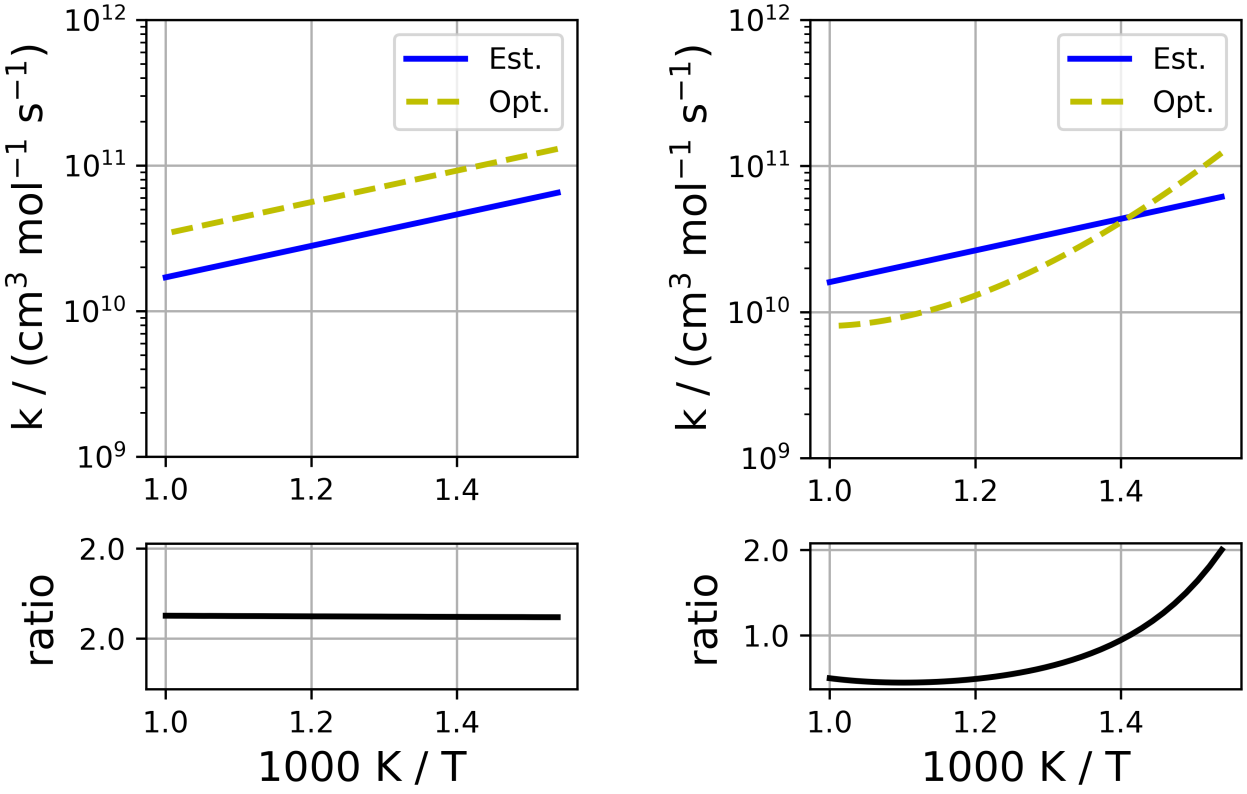

(c) $1\text{-}RO_2 + NO \rightleftharpoons 1\text{-}RO + NO_2$

(d) $2\text{-}RO_2 + NO \rightleftharpoons 2\text{-}RO + NO_2$

Fig. S18 Comparison of estimated and optimized rates for NO_x-cycling reactions of the form $RO_2 + NO \rightleftharpoons RO + NO_2$.

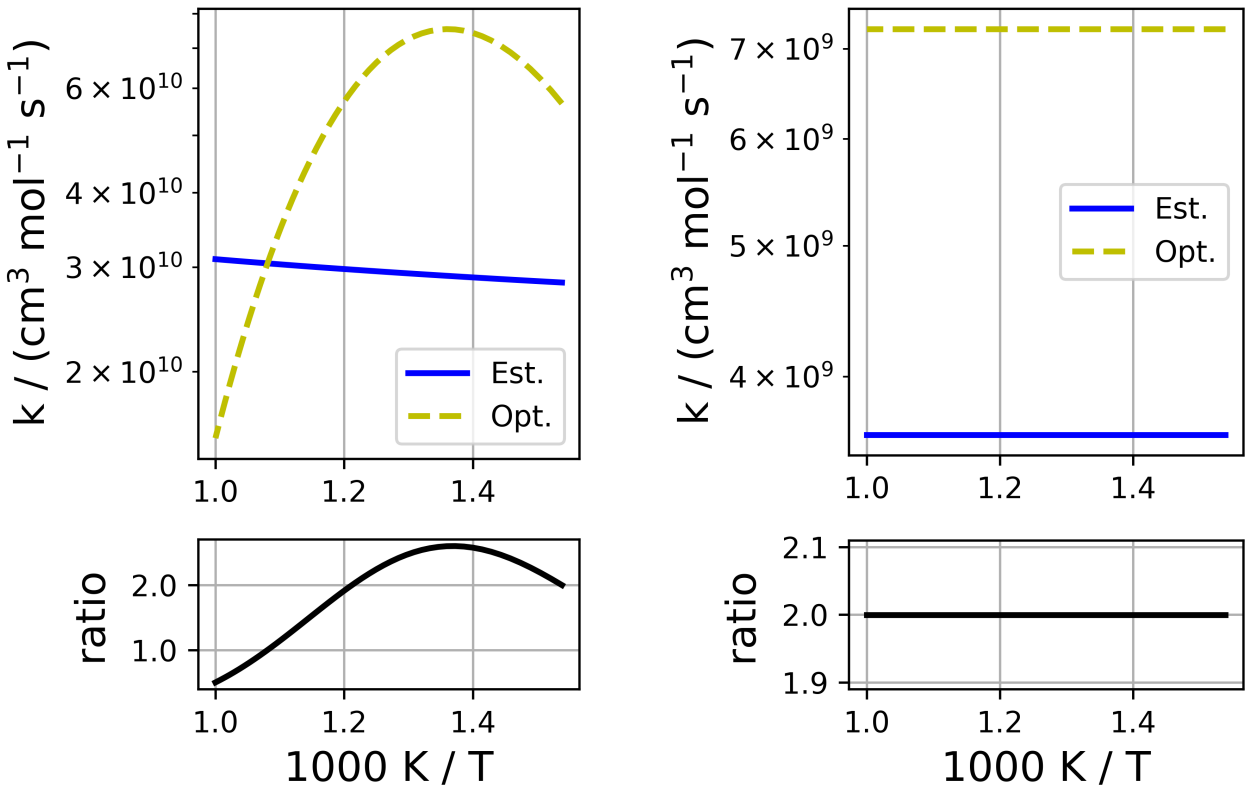

(a) $RO_2 + NO \rightleftarrows ROONO$

(b) $RO + NO_2 \rightleftarrows ROONO$

Fig. S19 Comparison of estimated and optimized rates for unimolecular product formation in competition with NO_x-cycling.